Electronic Supplementary Information for:

# Unconventional magnetism in the high pressure 'all transition metal' double perovskite $Mn_2NiReO_6$

Elena Solana-Madruga,[a] Khalid N. Alharbi, [a] Maria Herz, [a] Pascal Manuel,[b] and J.Paul Attfield [a]

## Supplementary Text:

### Experimental Procedures:

**Synthesis.** $Mn_2NiReO_6$ was prepared under high pressure and high temperature conditions. The precursor mixture was prepared by grinding in acetone stoichiometric proportions of MnO, NiO and $ReO_3$ reactants from Sigma-Aldrich (99.99%) and Alfa Aesar (99.9%). MnO and NiO were preheated at 1100 C under a $N_2$ flow in a tubular furnace. Repeated syntheses did not give phase pure samples, and the optimum samples were obtained when the precursor was packed into a Pt capsule and pressed under 8 GPa using a Walker module, heated to 1573 K for 20 minutes and quenched. Pressure was slowly released to ambient pressure.

**X-ray diffraction (XRD):** The synthesis product was checked using an in-house powder D2-Phaser Bruker X-ray diffractometer using Bragg-Brentano geometry for phase identification. Scans were collected at room temperature using Cu-$K_\alpha$ wavelength in the angular range $10 < 2\theta < 70$ º with a step size 0.033º for 30 sec /step and sample rotation. The experimental patterns were analysed with the Rietveld method (Fig. S1) using the FullProf suite toolbar [1].

**Neutron diffraction:** Neutron Powder diffraction (NPD) was measured using WISH beamline at ISIS facility. Several high pressure products were mixed together to give a ~50 mg sample. This was placed in a 4 mm V foil can for NPD data collection. Long scans were collected at 150, 75 and 1.5 K during 2.5 h to reach good statistics for structural characterization (100 μA total current). Shorter patterns were collected every 10 K on warming from 10 to 140 K during 35 min each (23.33 μA) to study the thermal evolution of the magnetic moments and lattice parameters. Rietveld fits on the long scans used data from banks 2-4. Bank 4 shows the magnetic peaks so fits to bank 4 are shown in the main text for comparison of the main magnetic peaks. Fits against banks 2 and 3 at 150 and 1.5 K are shown in Fig S2. Structure refinement results at 150 K are shown in Table S1. Magnetic symmetry analysis was performed using BasIreps tool implemented in the FullProf software. The resulting possible Irreducible Representations (Irreps) are summarized in Table S2.
In the case of the shorter scans, with lower statistics, bank 4 was selected to refine the minimum possible number of parameters. Equally separated experimental background points were selected, refined using an interpolation method in an initial step, and then fixed at each temperature. Zero shift, peak shape parameters, atomic positions and isotropic thermal factors were fixed from the refined values at 1.5 K for all phases. Overall thermal factors refined to oscillating but consistently increasing values with increasing temperature, and interpolated linear fit values (see Fig. S3) were fixed in the final fits for stability of the refined magnetic moments. $Ni^{2+}$ and $Re^{6+}$ magnetic moment components were constrained in a 2:1 ratio. Their refined direction in the *xz*-plane showed no thermal evolution within error so they are constrained to their refined 1.5 K orientation at all temperatures in the final model. Patterns collected at 150, 75 and 1.5 K was fitted using the same constraints to obtain consistent values for the reported thermal evolutions of lattice parameters, magnetic moments and $Mn^{2+}$ spin rotation in Fig. 4. These fits are shown in Fig S4 and the resulting refined parameters and magnetic moments are summarized in Tables S3 and S4 respectively.

**Magnetisation:** Magnetic susceptibility was measured using a Quantum Design XL-MPMS SQUID magnetometer under DC Zero-Field-Cooling (ZFC) and Field-Cooling (FC) conditions in the temperature range $2 < T < 300$ K under a magnetic field of 0.1 T. Magnetisation hysteresis loops were measured at 2, 60, 75 and 150 K, under applied magnetic fields up to 7 T.

### Supplementary discussion:

**Structural characterization:** Rietveld fits against XRD and NPD data confirm, as detailed in the main text, the formation of a monoclinic $Mn_2NiReO_6$ $P2_1/n$ double perovskite (DPv) structure with well ordered rock-salt B-site cations, in agreement with the large charge mismatch between $Ni^{2+}$ and $Re^{6+}$. Mn (A) and Re (B´) sites are occupied only by their respective cations, but 18% Mn substitutes for Ni, in keeping with the Ni-rich impurities observed. Secondary $ReO_2$, NiO and $Ni_{0.67}Mn_{0.33}O$ (17.8(6) %, 4.0(3) % and 12.2(2) % respectively) are included in the refinements. The two prior impurities are well known and

the latter, observed as a HP secondary phase elsewhere [2] fits both nuclear and magnetic peaks using a rock-salt structure with disordered Ni/Mn over the cation site. Its cell parameters and magnetic transition temperature agree with values interpolated between those of NiO and MnO. BVS calculations[3] of 2.5, 2.2 and 4.2 for Mn, Ni and Re respectively are consistent with the expected $Mn^{2+}{}_2Ni^{2+}Re^{6+}O_6$ charge distribution, allowing for the unreliablity of BVS estimates for distorted high pressure structures and especially for high formal oxidation states of Re.

The network of $NiO_6$ and $ReO_6$ octahedra accommodates the small A-site $Mn^{2+}$ cation (0.96 Å),[4] through tilts and internal distortions. The tilt angles, calculated from the half difference between the ideal 180° and the experimental <Ni-O-Re> angles along the *c* axis and within the *ab* plane are $\psi = 22.7(1)^o$ and $\theta = 24.5(1)^o$, respectively. Octahedral distortions, calculated from the B/B'-O bond lengths as $\Delta = 1/6 * \Sigma [(d_i - d_{Av})/d_{Av}]^2$, are 0.00156 and 0.00314 for $NiO_6$ and $ReO_6$ respectively, showing that both are highly distorted. The excess distortion for $ReO_6$ is consistent with a Jahn-Teller effect for $5d^1$ $Re^{6+}$ where 2 short and 4 long Re-O bonds are predicted and observed in Table S1.[5] The structure of $Mn_2NiReO_6$ thus displays an orbital ordering of the $Re^{6+}$ states, while $3d^8$ $Ni^{2+}$ is electronically non-degenerate.

To help understand why the structure of $Mn_2NiReO_6$ is so distorted, several relevant quantities (lattice strains $e_{ac} = 1 - \sqrt{2}a/c$ and $e_{bc} = 1 - \sqrt{2}b/c$, and the above tilt angles and octahedral distortion parameters) from all reported neutron diffraction studies of $Mn_2BB'O_6$ double perovskites are compared in Table S6. [3,5-9,13-15] All of these quantities would have zero values in an ideal cubic double perovskite structure, and so quantify the degree of structural distortion. In a simple $ABO_3$ perovskite, distortions generally increase as the tolerance factor $t = (r_A + r_O)/\sqrt{2}(r_B + r_O)$ based on ionic radii *r* decreases from *t* = 1. Larger average B,B' radius $r_{B,B'}$ (equivalent to smaller *t*) has some correlation with the measured distortions across the $Mn_2BB'O_6$ family, but the size difference $\Delta r_B = r_B - r_{B'}$ and electronic factors also contribute. $\Delta r_B$ is generally larger in $Mn_2B^{2+}B'^{6+}O_6$ than in $Mn_2B^{3+}B'^{5+}O_6$ materials, and this is seen to increase the $e_{bc}$ strain, although $e_{ac}$ is quite constant across both series. Jahn-Teller effects in $Re^{5+}$ and $Re^{6+}$ lead to greater ΔB' octahedral distortions than for non-degenerate $Sb^{5+}$ and $Te^{6+}$. Hence the discovery of the largest octahedral tilt angles and distortion parameters reported for this family to date in $Mn_2NiReO_6$ can be attributed to a combination of relatively large $\Delta r_B$ size difference and $Re^{6+}$ Jahn-Teller effect, rather than an exceptional average B,B' radius $r_{B,B'}$ and tolerance factor.

**Magnetic symmetry analysis:** Magnetic symmetry analysis performed with BasIreps tool implemented in the FullProf software, yields to 4 possible Irreps for Mn ($\Gamma_1$- $\Gamma_4$) and 2 for the B-site cations ($\Gamma_1$ and $\Gamma_3$), summarized in Table S2. Fits to the data showed that all three spins Mn, Ni and Re follow $\Gamma_1$ at all temperatures, with antiferromagnetic sublattices having non-zero refined $M_x$ and $M_z$ components. The weak ferromagnetic contribution observed from bulk magnetisation measurements is assigned to a small spin canting along the *y*-axis described by the parallel $M_y$ components allowed by Irrep $\Gamma_1$.

## Supplementary Figures:

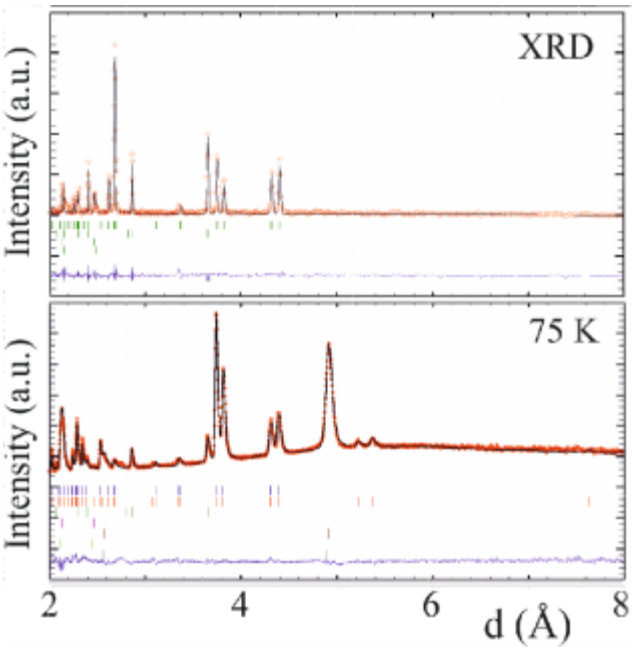


**Figure S1.** Rietveld fits to the XRD (top) and 75 K NPD (top) data.

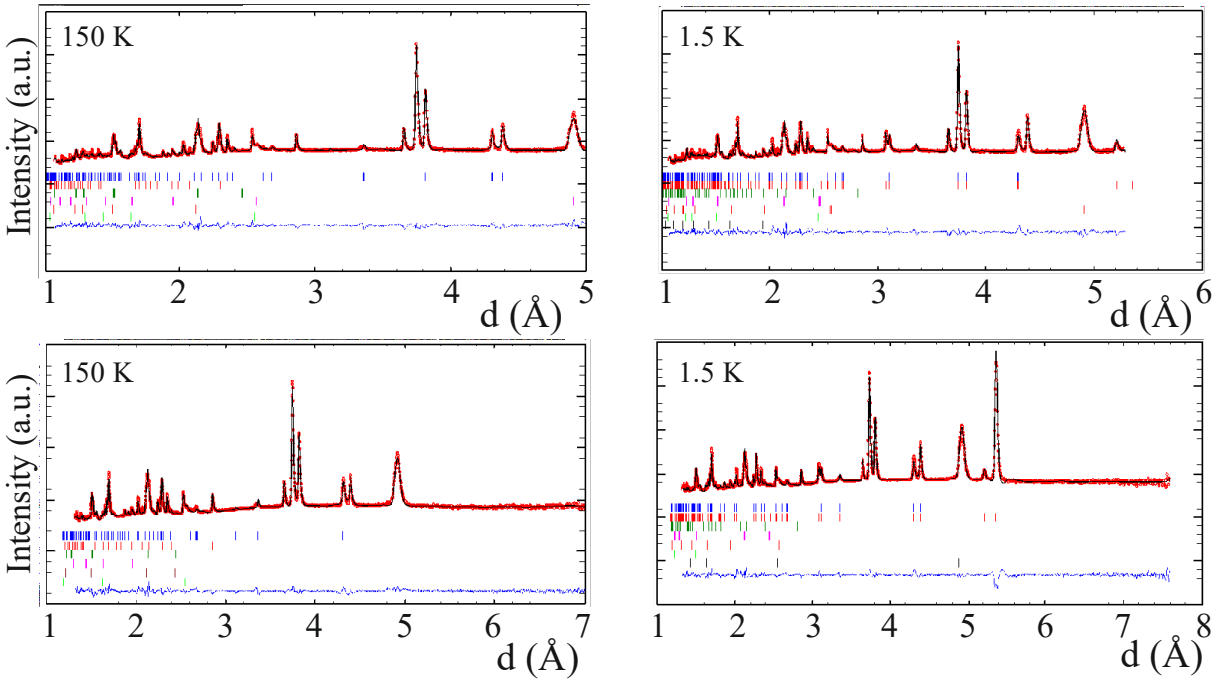


**Figure S2.** Rietveld fits to the NPD Banks 2 (top) and 3 (bottom) collected at 150 K (left) and 1.5 K (right).

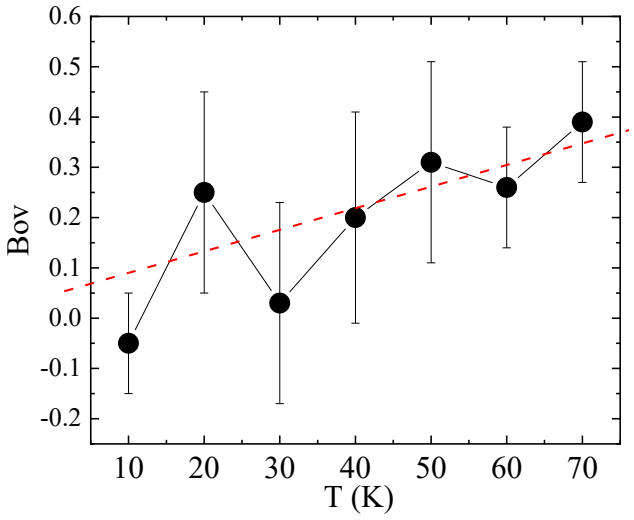


**Figure S3**. Overall thermal factor (in Å$^2$ units) refined from short scans at 10 – 70 K. Broken red line shows a linear fit.

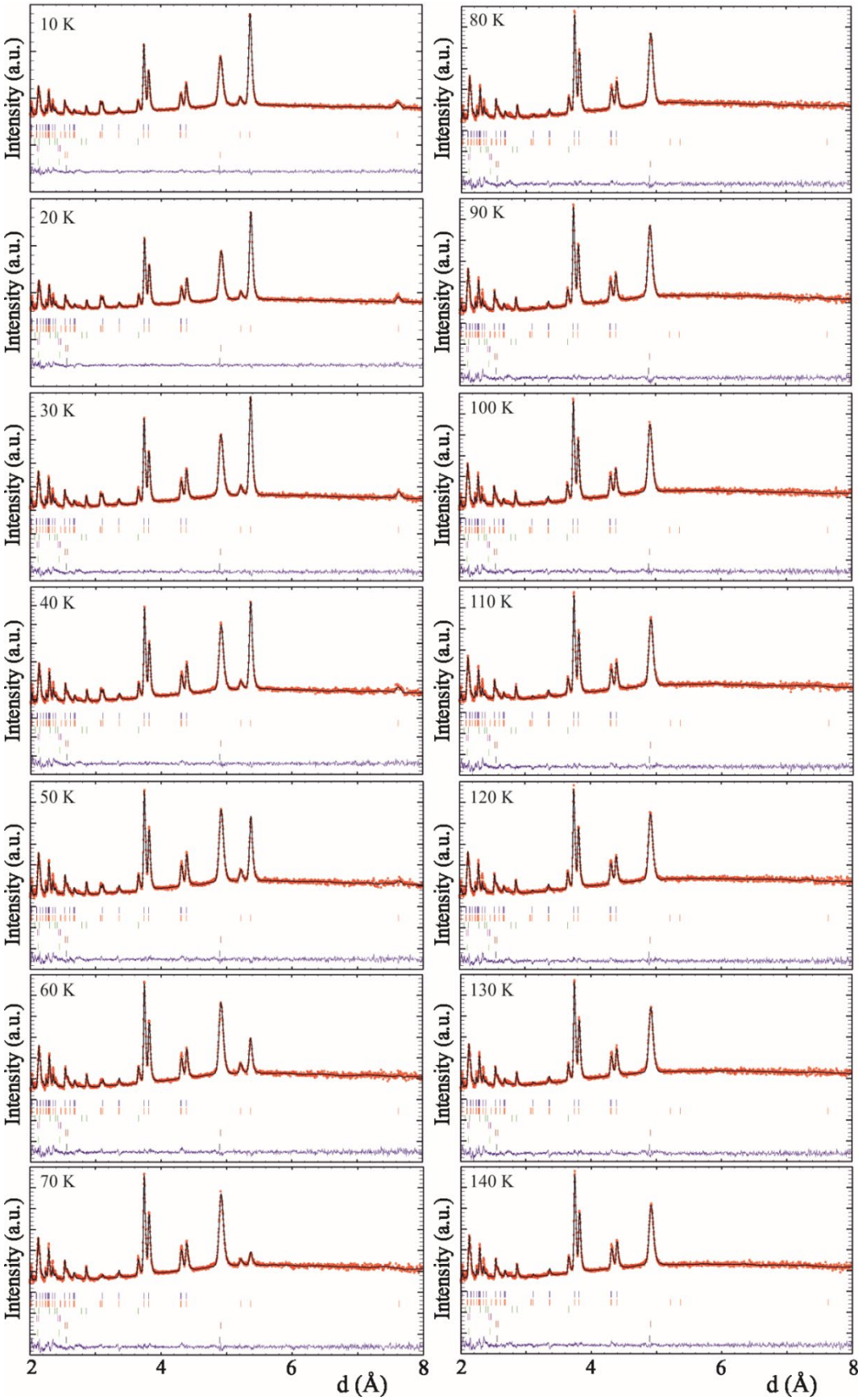


**Figure S4**. Rietveld fits to the NPD data (Bank 4) collected between 10 and 140 K.

## Supplementary Tables:

**Table S1.** Atomic coordinates and main interatomic distances and angles of $Mn_2NiReO_6$ from the Rietveld fit of 150 K NPD data using S.G. *$P2_1/n$*. Lattice parameters a = 5.2173(3) Å, b = 5.3664(3) Å, c = 7.6302(3) Å and β = 89.91(2)$^0$.

| Site | x | y | z | $U_{iso}$(Å$^2$) | Occ |
|---|---|---|---|---|---|
| Mn(4e) | 0.040(3) | 0.012(3) | 0.816(1) | 0.036(1) | 1.0 |
| Ni/Mn(2b) | 0.5 | 0.0 | 0.0 | 0.036 | 0.816/ 0.184(6) |
| Re(2c) | 0.0 | 0.5 | 0.0 | 0.036 | 1.0 |
| O1(4e) | 0.396(1) | 0.375(2) | 0.930(1) | 0.018(1) | 1.0 |
| O2(4e) | 0.296(1) | 0.290(2) | 0.572(1) | 0.018 | 1.0 |
| O3(4e) | 0.871(2) | 0.421(1) | 0.736(1) | 0.018 | 1.0 |
| 2x $d_{Ni-O1}$ (Å) | 2.15(1) | | 2x $d_{Re-O1}$ (Å) | 2.24(1) | |
| 2x $d_{Ni-O2}$ (Å) | 1.99(1) | | 2x $d_{Re-O2}$ (Å) | 1.96(1) | |
| 2x $d_{Ni-O3}$ (Å) | 1.97(1) | | 2x $d_{Re-O3}$ (Å) | 2.17(1) | |
| $<d_{Ni-O}>$(Å) | 2.04(1) | | $<d_{Re-O}>$(Å) | 2.12(1) | |

Fitting reliability factors: $R_p$ = 1.80%, $R_{wp}$ = 2.14%, $R_f$ =11.0%, $R_B$ = 11.0%, $\chi^2$ = 4.14.

**Table S2.** Basis vectors (BV) of the allowed Irreps for A and B magnetic sites of $Mn_2NiReO_6$ with propagation vector κ = [0 0 0]. Each BV shows $M_x$ $M_y$ $M_z$ components using + and – signs to indicate relative spin directions. x,y,z coordinate values for the cations are as shown in Table S1.

| Sym | $\Gamma_1$ | | $\Gamma_2$ | $\Gamma_3$ | | $\Gamma_4$ |
|---|---|---|---|---|---|---|
| | $BV_A$ | $BV_B$ | $BV_A$ | $BV_A$ | $BV_B$ | $BV_A$ |
| x,y,z | + + + | + + + | + + + | + + + | + + + | + + + |
| –x+1/2,y+1/2,–z+1/2 | – + – | | – + – | + – + | | + – + |
| –x,–y,–z | + + + | – + – | – – – | + + + | + – + | – – – |
| x+1/2,–y+1/2,z+1/2 | – + – | | + – + | + – + | | – + – |

**Table S3.** Refined lattice parameters and calculated strain (e) parameters with their estimated standard deviations (s).

| T(K) | a (Å) | $10^4$ sa | b (Å) | $10^4$ sb | c (Å) | $10^4$ sc | β (º) | $s_\beta$ | $10^4$ $e_{ac}$ | $10^4$ *$se_{ac}$ | $10^4$ $e_\beta$ | $10^4$ $se_\beta$ |
|---|---|---|---|---|---|---|---|---|---|---|---|---|
| 1.5 | 5.2147 | 2 | 5.3608 | 1 | 7.6211 | 3 | 89.99 | 0.01 | 334.9 | 1.170 | 1.597 | 2.243 |
| 10 | 5.2140 | 3 | 5.3618 | 3 | 7.6220 | 3 | 89.95 | 0.01 | 336.6 | 1.309 | 9.074 | 2.678 |
| 20 | 5.2140 | 3 | 5.3619 | 3 | 7.6219 | 3 | 89.95 | 0.01 | 336.6 | 1.190 | 9.011 | 2.575 |
| 30 | 5.2149 | 3 | 5.3618 | 1 | 7.6225 | 3 | 89.95 | 0.01 | 335.6 | 1.190 | 8.381 | 2.712 |
| 40 | 5.2147 | 3 | 5.3618 | 2 | 7.6229 | 3 | 89.9 | 0.01 | 336.5 | 1.229 | 16.9 | 2.918 |
| 50 | 5.2139 | 3 | 5.3628 | 2 | 7.6245 | 3 | 89.87 | 0.01 | 340.2 | 1.289 | 21.9 | 3.206 |
| 60 | 5.2140 | 4 | 5.3629 | 3 | 7.6258 | 3 | 89.84 | 0.01 | 341.8 | 1.408 | 26.9 | 3.272 |
| 70 | 5.2147 | 4 | 5.3631 | 5 | 7.6267 | 3 | 89.86 | 0.02 | 341.7 | 1.547 | 24.3 | 3.629 |
| 75 | 5.2150 | 4 | 5.3631 | 4 | 7.6276 | 3 | 89.81 | 0.01 | 342.8 | 1.369 | 33.0 | 2.790 |
| 80 | 5.2150 | 5 | 5.3638 | 5 | 7.6276 | 3 | 89.81 | 0.01 | 342.4 | 1.646 | 32.5 | 3.242 |
| 90 | 5.2153 | 5 | 5.3639 | 5 | 7.6280 | 3 | 89.82 | 0.01 | 342.3 | 1.646 | 32.3 | 3.261 |
| 100 | 5.2153 | 5 | 5.3642 | 5 | 7.6282 | 3 | 89.82 | 0.01 | 342.5 | 1.606 | 31.1 | 3.216 |
| 110 | 5.2158 | 5 | 5.3642 | 5 | 7.6287 | 4 | 89.84 | 0.02 | 342.2 | 1.838 | 28.3 | 3.472 |
| 120 | 5.2167 | 5 | 5.3645 | 5 | 7.6284 | 4 | 89.82 | 0.02 | 340.0 | 1.857 | 31.1 | 3.388 |
| 130 | 5.2167 | 5 | 5.3649 | 5 | 7.6292 | 4 | 89.84 | 0.02 | 341.2 | 1.857 | 28.2 | 3.563 |
| 140 | 5.2171 | 5 | 5.3662 | 5 | 7.6293 | 4 | 89.82 | 0.02 | 340.5 | 1.857 | 30.7 | 3.385 |
| 150 | 5.2183 | 4 | 5.3658 | 4 | 7.6305 | 3 | 89.84 | 0.01 | 339.7 | 1.447 | 27.2 | 2.945 |

**Table S4.** Refined magnetic moments and their contributions along the *x* and *z* axes, together with their estimated standard deviations (s).

| T(K) | Mn | | | | | | Ni | | | | | |
|---|---|---|---|---|---|---|---|---|---|---|---|---|
| | $m_x$ | $sm_x$ | $m_z$ | $sm_z$ | m | sm | $m_x$ | $sm_x$ | $m_z$ | $sm_z$ | m | sm |
| 1.5 | 3.31 | 0.03 | 2.21 | 0.03 | 3.98 | 0.03 | 0.737 | 0.0048 | 1.0046 | 0.0081 | 1.24595 | 0.00811 |
| 10 | 3.36 | 0.04 | 2.25 | 0.03 | 4.05 | 0.03714 | 0.7533 | 0.0208 | 1.006 | 0.0277 | 1.25678 | 0.0347 |
| 20 | 3.20 | 0.04 | 2.23 | 0.03 | 3.90 | 0.03703 | 0.78 | 0.021 | 1.0414 | 0.028 | 1.30112 | 0.03503 |
| 30 | 2.92 | 0.04 | 2.23 | 0.03 | 3.68 | 0.03658 | 0.7551 | 0.0217 | 1.0081 | 0.029 | 1.25954 | 0.0362 |
| 40 | 2.70 | 0.05 | 2.00 | 0.03 | 3.36 | 0.04397 | 0.6748 | 0.0238 | 0.9017 | 0.0317 | 1.12624 | 0.03972 |
| 50 | 2.18 | 0.06 | 1.89 | 0.03 | 2.89 | 0.04933 | 0.4333 | 0.0258 | 0.5791 | 0.0344 | 0.72326 | 0.04307 |
| 60 | 1.51 | 0.08 | 1.62 | 0.04 | 2.22 | 0.06175 | 0.2561 | 0.0313 | 0.3428 | 0.0417 | 0.4279 | 0.0523 |
| 70 | 0.72 | 0.18 | 1.2 | 0.06 | 1.40 | 0.1059 | 0.1257 | 0.0495 | 0.1695 | 0.066 | 0.21102 | 0.0831 |
| 75 | 0.57 | 0.18 | 0.93 | 0.05 | 1.10 | 0.10241 | 0.0672 | 0.0533 | 0.0896 | 0.071 | 0.112 | 0.08883 |

**Table S5.** Interatomic distances and angles from the Rietveld fit of $Mn_2NiReO_6$ DPv structure from 150 K NPD data.

| $d_{Mn-O1}$ (Å) | $d_{Mn-O2}$ (Å) | $d_{Mn-O3}$ (Å) |
|---|---|---|
| 2.05(2) | 1.70(1) | 2.24(1) |
| 2.83(3) | 2.56(1) | 2.44(1) |
| 3.10(1) | 2.73(3) | 3.14(1) |
| 3.64(2) | 3.81(1) | 3.35(2) |

| | <Ni-O-Re> ($^0$) | <Mn-O-Ni> ($^0$) | <Mn-O-Re> ($^0$) |
|---|---|---|---|
| O1 | 113.4(5) | 119.1(7) | 96.9(9) |
| O2 | 140.1(7) | 82.1(6)/97.6(9) | 85.0(6)/117.4(8) |
| O3 | 131.0(6) | 94.2(7)/106.6(6) | 82.6(6)/119.1(7) |

**Table S6. Interatomic** Averaged and difference ionic radii for B/B' cations, lattice strain parameters, octahedral tilt angles distortions (Δ) of $Mn_2BB'O_6$ double perovskites studied by NPD. References are in the final column.

| B, B' | $r_{B,B'}$, $\Delta r_B$ (Å) | ($e_{ac}$, $e_{bc}$) $*10^3$ | ψ, θ (º) | (ΔB, ΔB') $*10^5$ | Ref |
|---|---|---|---|---|---|
| $Sc^{3+}$, $Sb^{5+}$ | 0.67, 0.15 | 32.6, 0.07 | 20.5, 21.6 | 24.5, 1.37 | 6 |
| $Cr^{3+}$, $Sb^{5+}$ | 0.61, 0.02 | 27.4, 1.11 | 19.3, 20.2 | 26.7, 0.79 | 7 |
| $Fe^{3+}$, $Sb^{5+}$ | 0.62, 0.05 | 31.4, 1.89 | 19.4, 19.1 | 2.79, 3.16 | 8 |
| $Fe^{3+}$, $Re^{5+}$ | 0.61, 0.07 | 30.9, 0.98 | 20.3, 21.3 | 88.9, 263 | 9 |
| $Mn^{2+}$, $Re^{6+}$ | 0.69, 0.28 | 33.2, 11.9 | 20.5, 22.4 | 52.5, 35.8 | 10 |
| $Co^{2+}$, $Re^{6+}$ | 0.65, 0.20 | 30.0, 8.11 | 20.8, 20.9 | 70.7, 7.08 | 11 |
| $Ni^{2+}$, $Re^{6+}$ | 0.62, 0.14 | 33.0, 5.33 | 22.7, 24.5 | 156, 314 | a) |
| $Mn^{2+}$, $Te^{6+}$ | 0.70, 0.27 | 41.3, 12.6 | 19.7, 21.5 | 134, 5.54 | 12 |

a) This work.

## References


1. J. Rodriguez-Carvajal, *Physica B*, **1993**, *192*, 55.
2. E. Solana-Madruga, Y. Sun, A. M. Arévalo-López, J. P. Attfield, *Chem. Commun.*, **2019**, *55*, 2605-2608.
3. J. P. Attfield, *Solid State Sci.*, 2006, **8**, 861–867.
4. R. D. Shannon, C. T. Prewitt, *Acta Cryst. B*, 1969, **25**, 925–946.
5. C. A. Marjerrison, C. M. Thompson, G. Sala, D. D. Maharaj, E. Kermarrec, Y. Cai, A. M. Hallas, M. N. Wilson, T. J. S. Munsie, G. E. Granroth, R. Flacau, J. E. Greedan, B. D. Gaulin, G. M. Luke. *Inorg. Chem.* 2016, **55**, 10701−10713.
6. E. Solana-Madruga, A. J. Dos santos-García, A. M. Arévalo-López, D. Ávila-Brande, C. Ritter, J. P. Attfield, R. Sáez-Puche. *Dalton Trans.* 2015, **44**, 20441-20448.
7. A. J. Dos santos-García, E. Solana-Madruga, C. Ritter, D. Ávila-Brande, O.Fabelo, R. Sáez-Puche. *Dalton Trans.* 2015, **44**, 10665-10672.
8. A. J. Dos santos-García, C. Ritter, E. Solana-Madruga, R. Sáez-Puche, *J. Phys. Condens. Matter.,* 2013, **25**, 206004.
9. A. M. Arévalo-López, G. M. McNally, J. P. Attfield, *Angew. Chem. Int. Ed.* 2015, **54**, 12074 –12077.
10. A. M. Arévalo-López, F. Stegemann, J. P. Attfield, *Chem. Commun.*, 2016, **52**, 5558.

11. C. E. Frank, E. E. McCabe, F. Orlandi, P. Manuel, X. Tan, Z. Deng, M. Croft, V. Cascos, T. Emge, H. L. Feng, S. Lapidus, C. Jin, M. X. Wu, M. R. Li, S. Ehrlich, S. Khalid, N. Quackenbush, S. Yu, D. Walker, M. Greenblatt, *Chem. Commun.*, 2019, **55**, 3331.
12. A. M. Arévalo-López, E. Solana-Madruga, C. Aguilar-Maldonado, C. Ritter, O. Mentré, J. P. Attfield. *Chem. Comm.* 2019, **55**, 14470-14473.

## Author Contributions

All authors contributed significantly to this study. ESM, KNA and MH performed sample synthesis and characterization; NPD data were collected by ESM, KNA and PM and analysed by ESM and KNA; the manuscript was prepared by ESM, KNA and JPA with comments from PM; JPA supervised the study.